Silicon (2022) 14:6233–6243
https://doi.org/10.1007/s12633-021-01329-4

ORIGINAL PAPER

Green Synthesis for MCM-41 and SBA-15 Silica Using the Waste Mother Liquor

Thianne Silva Batista Barbosa[1] · Thiago Rodrigo Barbosa Barros[1] · Tellys Lins Almeida Barbosa[1] · Meiry Gláucia Freire Rodrigues[1]

Received: 15 April 2021 / Accepted: 15 August 2021 / Published online: 26 September 2021

Abstract

In an attempt to synthesize silicas with respect to green chemistry, the synthesis of MCM-41 and SBA-15 silicas by a low-cost approach through the recycling of waste mother liquors was investigated. The addition of the mother liquor in consecutive syntheses was carried out in order to evaluate the different effects on the physical and chemical properties of the silicas. MCM-41 silicas were characterized by X-ray diffraction, which confirmed the formation of the hexagonal phase in the mother liquor used. According to the results of XRD, BET and SEM, SBA-15 silica has a structure that includes mesopores of various levels, crystallites and grains within the original particles. From the analysis of the textural characteristics of the various samples obtained through nitrogen adsorption/desorption studies carried out at -196 °C, the following conclusions can be highlighted: (i) For the synthesis of MCM-41, there was a trend of increase in specific surface areas, reduction in pore diameter and increase in wall thickness; (ii) For the synthesis of SBA-15 there was an increase in the specific surface area, an increase in the pore diameter and a reduction in the wall thickness. It was found that, under the synthesis conditions, the mother liquor user had an influence on the final characteristics of these materials.

Keywords MCM-41 · Synthesis · SBA-15 · Mother liquor recycling · Green synthesis · Environmentally friendly

1 Introduction

Mesoporous materials are a class of solids that have uniform pore sizes (1.5 to 40 nm), large surface areas (up to 2500 m^2.g-1), large pore volumes, excellent thermal stability, and structures that can be modified in different ways [1]. These materials are of great interest, mainly as catalysts [2] and adsorbents [3]. The mesostructured molecular sieves in the 2D group (MCM-41 and SBA-15) have hexagonal symmetry and are easier to produce than those of other groups [4]. Several models have been proposed to explain the formation of mesoporous materials that provide a rational basis for the various synthesis routes. In general, these models are based on the presence of surfactants in a solution that guide the formation of the inorganic mesostructure [5, 6].

The typical synthesis process for MCM-41 involves reagents such as: the silicon source, which serves to build the structure of the walls of the mesoporous material, the most commonly-used being pyrolyzed silica (Aerosil), tetraethyl orthosilicate (TEOS), and sodium silicate; surfactants, which are molecules with hydrophilic and hydrophobic characteristics that serve to guide the formation of the mesoporous structure, with cetyltrimethylammonium (CTAB) in chloride, bromide, or hydroxide form being the most commonly-used [7]; the hydroxyl source, which provide the organic cation that assists in the formation of basic silica construction units, with the most commonly-used being tetramethylammonium hydroxide (TMAOH) and ammonium hydroxide (NH_4OH) [8].

The SBA-15 silica is synthesized in an acidic medium with the use of cationic surfactants, a nonionic oligomeric or triblock copolymer, and directing agent for highly-ordered porous crystal structures. Conventional synthesis of SBA-15 is also performed using tetraethylorthosilicate (TEOS), tetramethylorthosilicate (TMOS), or sodium silicate as a silica source [9].

During the synthesis of these materials, the desired solid crystals are separated from the reaction mixture and the filtrate

✉ Meiry Gláucia Freire Rodrigues
meirygfr@hotmail.com

[1] Academic Unit of Chemical Engineering, Federal University of Campina Grande, Av. Aprígio Veloso, 882 - Bodocongó, Campina Grande, PB 58109-970, Brazil

(mother liquor), which is rich in organic and inorganic species, is often unusable [10, 11]. The direct disposal of the mother liquor will not only lead to the waste of raw materials, but can also cause environmental pollution [12]. Some authors address the reuse and recycling of mother liquor as a raw material for the syntheses of porous materials [13–18]. To make synthesis processes more attractive, the principles of green chemistry have been implemented as concepts and actions related to economy, sustainability of resources, and environmental protection [19]. The Twelve Principles of Green Chemistry are "rules" that help chemists achieve the goal of sustainability and are characterized by careful planning of chemical synthesis processes in order to reduce adverse consequences [20].

This study aims to reuse the mother liquor in two subsequent syntheses of the SBA-15 and MCM-41 silicas to assess any possible changes in the physical, chemical, and morphological properties of each material.

2 Materials and Methods

2.1 Materials

Poly(ethylene glycol)block-poly(propylene glycol)block-poly(ethylene glycol) copolymer (Pluronic P123, PEG, 30 %), cetyltrimethylammonium bromide (CTAB, 98 %), hydrochloric acid (HCl, 37 %), ammonium hydroxide (NH_4OH, 29 %) and tetraethylorthosilicate (TEOS, 98 %) were purchased from SIGMA-ALDRICH (MERCK).

2.2 Synthesis of Silicas MCM-41 and SBA − 15 Using Mother Liquor

Tables 1 and 2 show the masses used to prepare the **silicas** MCM-41 and SBA-15.

Table 3 shows the results of chemical analysis of the mother liquor of MCM-41 1G.

The MCM-41 1G silica was conventionally synthesized using the hydrothermal method, according to the procedure described by authors [8]. This synthesis consisted of dissolving the CTAB (structure-directing agent) in deionized water at 50 °C under agitation for 30 min. The solution was cooled to approximately 25 °C and NH_4OH was added under stirring at room temperature for 15 min. Then, the TEOS silica source was slowly added to the reaction medium and kept under stirring for 2 h. The gel obtained was placed in autoclaves and heated in an oven at 30 °C for 24 h.

Table 1 Masses used in the syntheses of MCM-41

Material/ component (g)	MCM-41 1G	MCM-41 2G	MCM-41 3G
SiO_2	6.72	6.72	6.72
CTAB	3.53	3.53	3.53
NH_3	6.04	6.04	6.04
H_2O	68.91	-	-
Mother liquor	-	68.91	68.91
Solid yield (g)	12.50	12.00	12.00

Table 2 Masses used in the syntheses of SBA-15

Material/ component (g)	MCM-41 1G	MCM-41 2G	MCM-41 3G
SiO_2	5.22	5.22	5.22
CTAB	2.47	2.47	2.47
HCl	14.08	14.08	14.08
H_2O	78.22	-	-
Mother liquor	-	78.22	78.22
Solid yield (g)	11.00	9.00	9.00

The conventional synthesis of the SBA-15 1G silica was based on the methodology described by authors [9]. The Pluronic P123 surfactant was dissolved in concentrated HCl and water, under stirring and heated at 35 ºC for 4 h. Following this, TEOS was added and the synthesis was aged under agitation and heated at 35 ºC for 24 h. The material was then taken to the oven for hydrothermal treatment at 100 °C for 48 h in a teflon crucible wrapped in a stainless-steel autoclave.

After crystallization, the as-prepared materials were separated by filtration into raw MCM-41 or SBA-15 and mother liquor. Figure 1 show the flow diagram synthesis of MCM-41 and SBA-15. Silicas were dried in an oven at 60 °C for 24 h, after which they were subjected to the calcination process in a muffle furnace at 550 °C for 7 h with a heating ramp of 5 °C.min^{-1} to remove the organic template.

The syntheses of the materials in consecutive generations (MCM-41 2G; MCM-41 3G; SBA-15 2G; and SBA-15 3G) occurred similarly to the procedures already described. However, the mother liquor (ML) collected in traditional hydrothermal synthesis of silicas (MCM-41 1G or SBA-15 1G) was added during the initial stage of the synthesis without modifications, replacing the mass corresponding to the water needed to form the reaction mixture. The reaction mixtures and the molar composition of each material can be seen in Table 4.

In Fig. 1 is shown flow diagram synthesis of silicas.

Table 3 Chemical analyses of mother liquor of MCM-41 1G

Parameter (mg.L^{-1})	Result
SiO_2	820.2
Ammonium (NH_3)	1027.24

2.3 Characterizations

For the characterization of the synthesized and calcined samples by XRD (X-ray diffraction), a Shimadzu XRD-6000 diffractometer was used, with CuKα radiation, a voltage of 40 KV, a current of 30 mA, a step size of 0.020 and a time per step of 0.60 s, with a sweep speed of 2º per minute and 2θ angle ranging from 1° to 10°. To obtain the infrared, IR VERTEX 70 equipment from BRUKER was used. The samples in the form of tablets were dried in an oven in advance and placed in the sample holder. The IR spectra were obtained at wavelengths in the 400–4000 cm^{-1} range with a resolution of 4 cm^{-1}. To identify and quantify the chemical composition of the synthesized samples, an S2 Ranger Bruker dispersive energy X-ray spectrophotometer was used. To perform microscopy on the samples a VEGA TESCAN scanning electron microscope was used. The powder samples were covered with a thin layer of gold by a metallizer and fixed to a support with carbon adhesive tape. Thermogravimetric analysis was performed in a Shimadzu DTG-60 H Thermal Analyzer in a nitrogen atmosphere with a gas flow of 50 $mL.min^{-1}$. The sample was heated from room temperature up to 1000 °C, at a heating rate of 10 $°C.min^{-1}$. Ammonia analysis was determined according to the Standard Test Methods for Ammonia Nitrogen in Water (ASTM D 1426). Silica analysis was determined according to the Standard Test Method for Silica in Water (ASTM D859-16).

3 Results and Discussion

3.1 Characterization of Raw Materials

Figure 2(a) shows the diffractograms of the samples of MCM-41 synthesized initially (MCM-41 1G) and from the following generations MCM-41 2G and MCM-41 3G. The diffractograms of the synthesized SBA-15 samples (SBA-15 1G, SBA-15 2G and SBA-15 3G) are shown in Fig. 2(b).

According to authors [7, 8], the X-ray diffractograms in Fig. 2(a) show that the materials obtained are characteristic of the MCM-41 silica in all three generations. The XRD's of the synthesized MCM-41 molecular sieves show an intense peak at 2θ = 2.2°, corresponding to the (1 0 0) plane and two to three smaller peaks between 3.5° and 6.0° due to the (1 1 0), (2 0 0), and (2 1 0) planes, indicating the presence of ordered mesoporous hexagonal MCM-41 [19, 21, 22]. A decrease in intensity for the first peak and the disappearance of the last peak for the samples MCM-41 2G and MCM-41 3G in relation to MCM-41 1G can be observed. Due to the substances present in the mother liquor (SiO_2, NH_3), this decrease in pore ordering can be attributed to the pH variation that occurs when it is added to the reaction mixture and also the CTAB/SiO_2 ratio [18]. The diffractograms (Fig. 2a) indicate that the positions of the peaks (100) of MCM-41 1G, MCM-41 2G and MCM-41 3G were gradually changed to lower 2 theta values suggesting an increase in wall thickness (see Table 6).

Table 4 Molar composition used in the synthesis of each material

Material	Molar Composition
MCM-41	1.0 SiO_2: 0.3 CTAB: 11 NH_3: 144 H_2O
SBA-15	1.0 SiO_2: 0.017 P_{123}: 5.7 HCl: 193 H_2O

According to what was described by authors [9], the diffractograms in Fig. 2(b) show that the synthesized materials are characteristic of the SBA-15 silica. Note the presence of three well-defined peaks in all generations, which indicates a good uniformity of materials. The presence of the first reflection peak of the (1 0 0) plane at 2θ = 0.9° and of the (1 1 0) and (2 0 0) planes at 2θ = 1.6° and 1.8°, respectively, preserve the characteristic patterns of the SBA-15 mesostructure with reflections associated with a p6mm hexagonal symmetry of the mesoporous material [9, 22–24].

The chemical analysis of the silicas is presented in Table 5. Chemical analyses of all generations of MCM-41 obtained through ED-XRF showed a high content of silicon dioxide SiO_2 (99.85 wt%, 99.46 wt%, and 99.52 wt% in the first, second, and third generations, respectively) in the compositions as reported by authors [25]. Chemical analyses determined through ED-XRF of the synthesized SBA-15 silicas (SBA-15 1G, SBA-15 2G, and SBA-15 3G) indicate that SBA-15 is composed essentially of SiO_2 (100.00 wt%, 99.97 wt%, and 99.99 wt% in the first, second and third generations, respectively). These samples appeared to be chemically pure because they did not present impurities. Samples of the SBA-15 molecular sieve consisting only of Si and O were observed in the study by authors [26].

The spectra of the synthesized (MCM-41 1G, MCM-41 2G, and MCM-41 3G) and calcined (MCM-41 1G Cal, MCM-41 2G Cal, and MCM-41 3G Cal) samples are shown in Fig. 3(a) and (b), respectively. The spectra of the synthesized (SBA-15 1G, SBA-15 2G, and SBA-15 3G) and calcined (SBA-15 1G Cal, SBA-15 2G Cal, and SBA-15 3G Cal) samples are shown in the Fig. 3(c) and (d), respectively.

The spectra of the synthesized and calcined MCM-41 samples from all generations, presented in Fig. 3(a), (b), (c), and (d), show bands in the 500–4000 cm^{-1} region that are characteristic of the fundamental vibrations of the functional groups present in the structures of molecular sieves MCM-41 and SBA-15 [27]. In Fig. 3(a) and (b), the spectra have bands between 920 and 950 cm^{-1} corresponding to the angular vibrations of the Si-OH bond of the silanol groups existing in the MCM-41 structure. In the 1000–1250 cm^{-1} region, it is possible to observe the presence of a broad band composed of two other bands, a main band at 1050 and

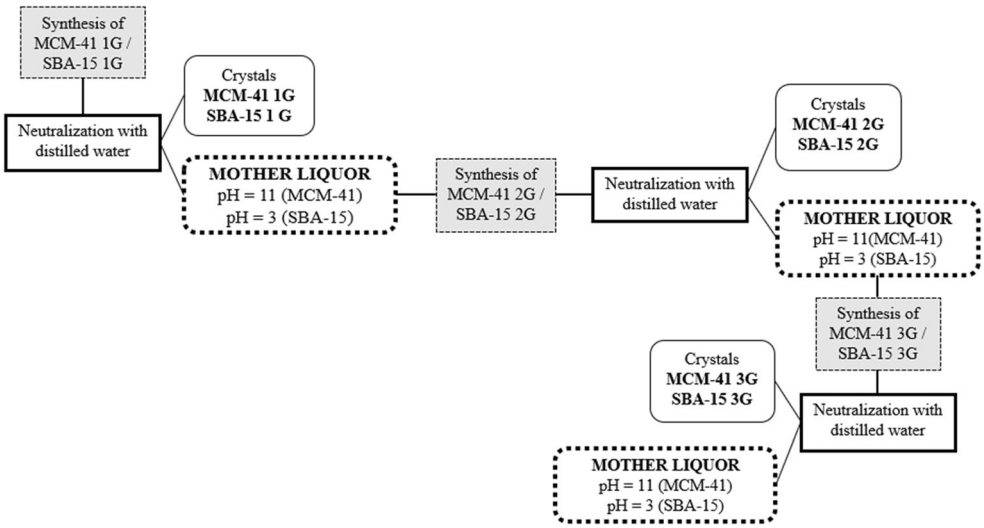

Fig. 1 Flow diagram synthesis of silicas

1066 cm^{-1} and a less-developed secondary band at 1025 and 1190 cm^{-1}. These correspond to asymmetric stretching of the Si-O-Si bond [18, 27]. In the spectra of the non-calcined samples, the vibrational bands at 1465 cm^{-1} and 2920 cm^{-1} are attributed to stretching between the CH of the CH_2 and CH_3 groups that correspond to the presence of the salt CTAB, which is occluded in the MCM-41 pores [28, 29].

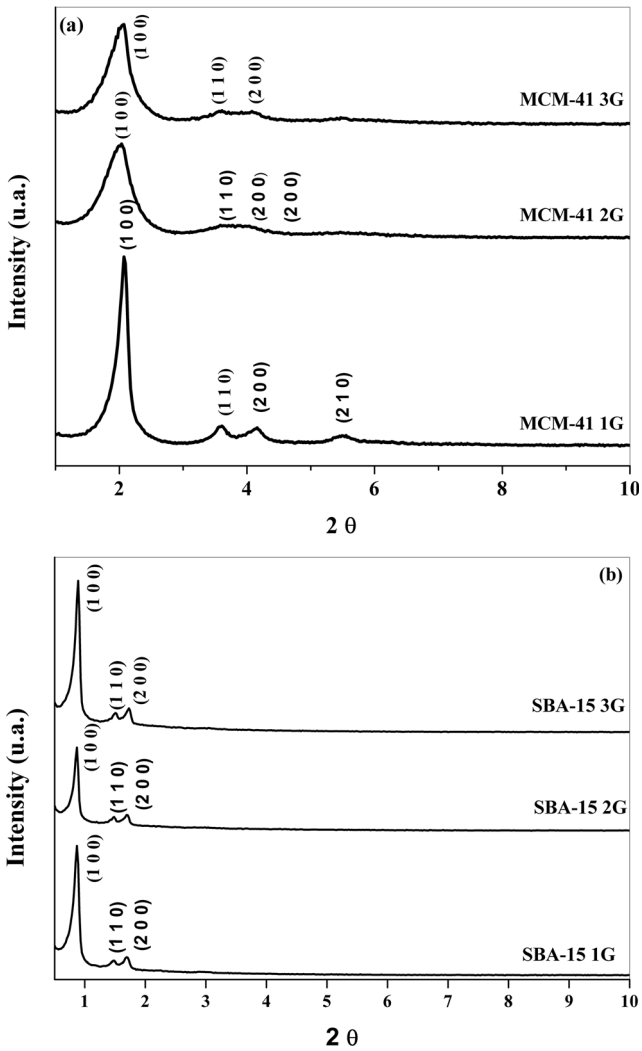

Fig. 2 X-ray diffractograms of the MCM-41 (**a**) SBA-15 (**b**)

The spectra of the synthesized and calcined SBA-15 samples presented in Fig. 3(c) and (d) show a band around 787–850 cm^{-1} that corresponds to the symmetrical stretching of the Si-O-Si bond, very common in MCM-41 and SBA-15 type materials [28]. Another band at 930–1010 cm^{-1} corresponds to the angular vibration of the Si-OH bond of the silanol groups in the SBA-15 structure. In the 1065–1270 cm^{-1} region, it is possible to observe the presence of wide bands at 1065, 1070, and 1150 cm^{-1} and other less-developed bands at 1220, 1270 and 1205 cm^{-1}, in the first, second, and third generation samples, respectively. In the calcined samples, the main bands are at 1060, 1050, and 1060 cm^{-1} and the secondary bands are at 1211, 1211, and 1203 cm^{-1}, in the first, second, and third generation samples, respectively. These values all correspond to asymmetric stretching of the Si-O-Si bond [30]. In the spectra of the non-calcined samples, the vibrational bands at around 2890, 2969, and 2885 cm^{-1} refer to the vibrations of the organic molecule of the Pluronic P123 template due to the stretching

Table 5 Chemical composition of the silicas

Material	Composition (wt%) SiO_2
MCM-41 1G	99.85
MCM-41 2G	99.46
MCM-41 3G	99.52
SBA-15 1G	100.00
SBA-15 2G	99.97
SBA-15 3G	99.99

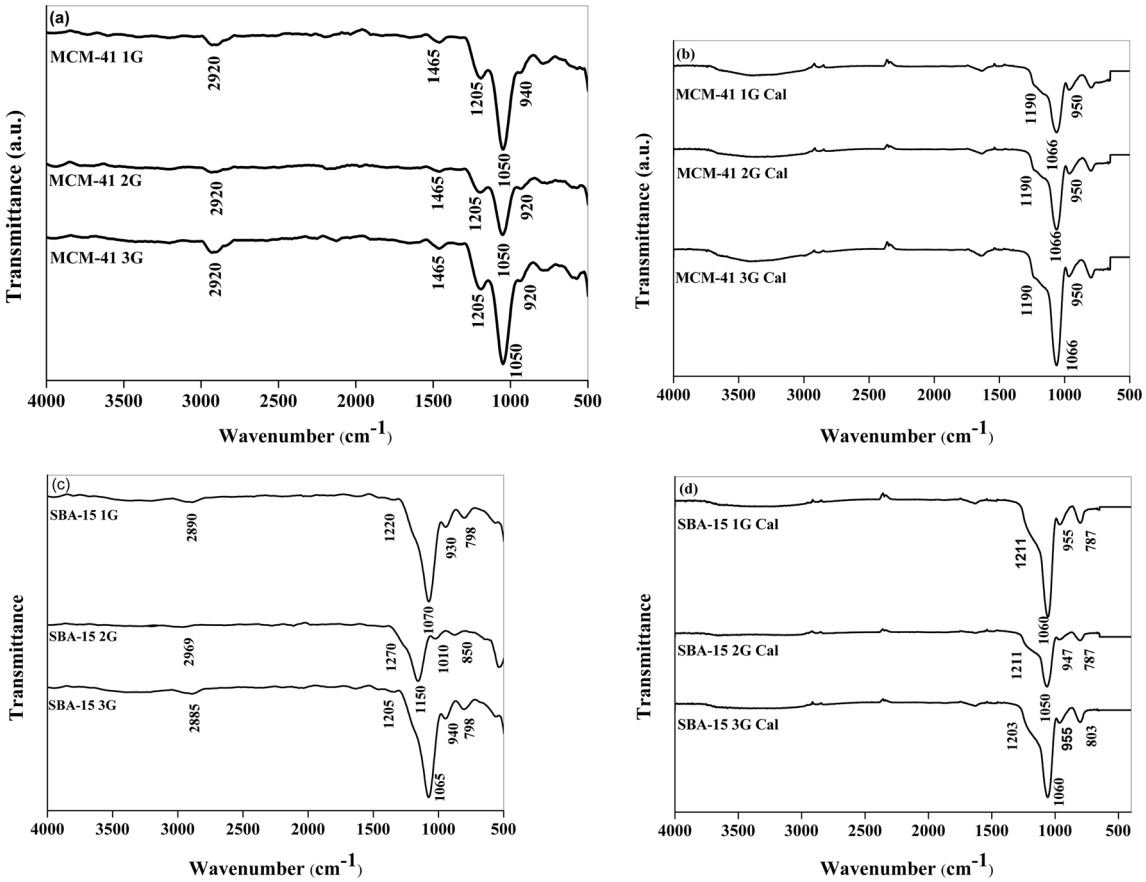

Fig. 3 FTIR spectra of the silica samples (**a**) MCM-41 (**b**) MCM-41 Cal (**c**) SBA-15 (**d**) SBA-15 Cal

in the CH bonds of the CH_2 and CH_3 groups [31, 32]. After calcination, these bands disappear, indicating the removal of the surfactant from the material structure [33].

Figure 4 shows the images obtained through SEM for the synthesized MCM-41 samples (MCM-41 1G, MCM-41 2G, and MCM-41 3G) and synthesized SBA-15 samples (SBA-15 1G, SBA-15 2G, and SBA-15 3G).

The morphologies presented by the MCM-41 and SBA-15 silicas can be diverse and are directly dependent on the synthesis conditions, such as: agitation, pH, aging temperature, hydrothermal synthesis temperature, aging time, and hydrothermal synthesis time, among others [34]. According to Fig. 4, the micrographs obtained through SEM of the synthesized MCM-41 samples show a morphology similar to those found by authors [35] who synthesized MCM-41 using NH_4OH at different temperatures. The particles have irregular and non-uniform spherical clusters in all generations [36]. In Fig. 4, the SBA-15 micrographs show nanochannels that are well-ordered and aligned with the direction of the fibers for samples from the three generations. They present similar morphologies to those found by [5, 37], with micrometric silica fibers formed from the linear adhesion of nodules of submicrometric particles, giving the appearance of interlaced bead necklaces [38].

Figure 5(a) show the adsorption and desorption isotherms of the calcined MCM-41, respectively, obtained through the BET method [39]. Initially, nitrogen adsorption occurs on the material surface at a relative pressure (P/P_0) below 0.2. After the monolayer is formed, multi-layers develop over it. From a (P / P0) of 0.4, there is no hysteresis. This behavior may have been a function of the treatment temperature (350 °C) of the sample during the physical adsorption analysis of N_2 [39]. Possibly there was a collapse of the sample due to the low resistance to activation at high temperature. This behavior is observed for all generations of the samples. In the final part of the isotherm, after capillary condensation, the pore is saturated and a small amount of N_2 is adsorbed on the outer walls, resulting in a maximum volume of adsorbed gas of approximately 450, 430, and 410 $cm^3.g^{-1}$ for MCM-41 1G, 2G, and 3G, respectively.

Figure 6(a) show the N_2 adsorption/desorption isotherms at -196 °C of the calcined SBA-15. The isotherms for the calcined SBA-15 sample were of type IV and exhibited a welldefined H1 hysteresis loop according to the IUPAC classification relative to the mesoporous materials [5].

For SBA-15 these values are 500, 540, and 595 $cm^3.g^{-1}$ in the first, second, and third generations, respectively. The isotherm for the MCM-41 sample exhibited H4 type hysteresis, corresponding to porous materials made up of narrow, slit-

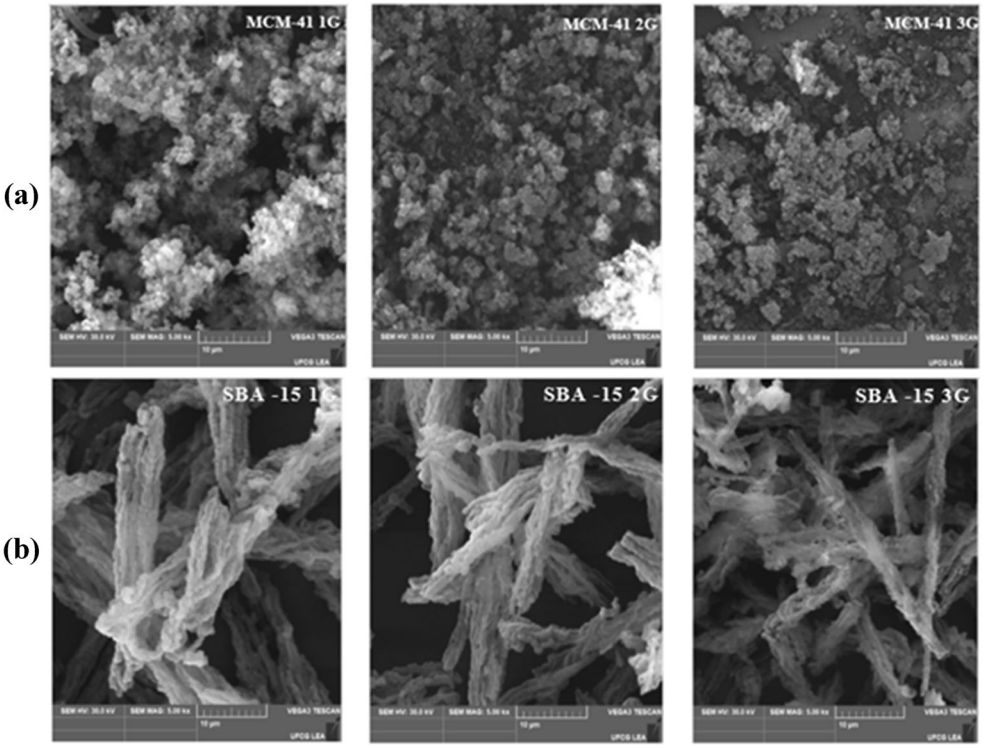

Fig. 4 Micrographs of the silica samples (**a**) MCM-41 (**b**) SBA-15

shaped pores. For SBA-15, the isotherm showed hysteresis of type H1 [36] associated with porous materials that consist of agglomerates or compact groups of uniform spheres in a regular arrangement and, therefore, have narrow pore size distributions.

The graphs of the pore distributions of the MCM-41 and SBA-15 samples, as obtained through the BJH method, are shown in Fig. 5(b) and 6(b), respectively.

The pore diameter distribution in Fig. 5(a) showed peaks between 2 and 3 nm for the three generations of MCM-41, which are attributed to the microporous region, and also a peak at 3.6 nm in the first generation only, which is attributed to the mesoporous region. The pore diameter distribution (Fig. 6b) showed showed all peaks of the three sample generations to be between 6 and 7 nm, all attributed to the micropore region.

According to Table 6, the BET surface area of MCM-41 1G was 726 $m^2.g^{-1}$ and for the following generations this value increased to 818 and 867 $m^2.g^{-1}$ for MCM-41 2G and MCM-41 3G, respectively. The values of BET surface area found are lower than the values found in the literature [22]. For the pore wall thickness of the MCM-41 structures, a similar behavior can be seen, in which the values increased in the following generations, to 2 and 2.22 in the second and third generations, respectively. These values are higher than those found in the literature [5], which indicates standard values of Wt (nm) for MCM-41 between 1 and 1.5 nm.

Table 6 shows the values obtained for the network parameter, a_0 (nm), which can be calculated in a simplified manner, $a_0 = 2d_{100}(3^{1/2})^{-1}$, where d_{100} corresponds to the interplanar distance of the (1 0 0) diffraction plane; the surface area, S_{BET} ($m^2.g^{-1}$), obtained by the BET method; and the average pore diameter, Dp (nm), obtained by the BJH method. Vp ($cm^3.g^{-1}$) corresponds to the pore volume of the samples and W_t corresponds to the nanometer thickness of the structural wall, calculated as the difference between the network parameter a_0 and the pore diameter, Dp [40].

The BET surface area for the SBA-15 samples also increased in subsequent generations, starting from 550 $m^2.g^{-1}$ for the first generation and reaching 600 $m^2.g^{-1}$ by the last generation of the synthesis. The wall thicknesses for the SBA-15 samples were around 6 nm for the first and second generation, with a small drop in the third generation to 5.51 nm. However, there is slight differences with that found in the literature [5] and indicate a greater thermal and hydrothermal stability than that to MCM-41. All BET surface area values for samples MCM-41 and SBA-15 are lower than those found in the literature [22, 41, 42].

The thermogravimetric analysis of the synthesized MCM-41 (MCM-41 1G, MCM-41 2G, and MCM-41 3G) and SBA-15 (SBA-15 1G, SBA-15 2G, and SBA-15 3G) samples are shown in Fig. 7(a) and (b), respectively.

From the thermogravimetric curves of the samples of the synthesized MCM-41 represented in Fig. 7(a), three mass loss events can be observed for all samples. The first event below 150 °C related to the desorption of physiosorbed water in the pores of the MCM-41 that corresponds to 4 % of loss of mass. The second in the range of 150–320 °C attributed to the decomposition of the template (CTAB), i.e., the Hoffmann elimination

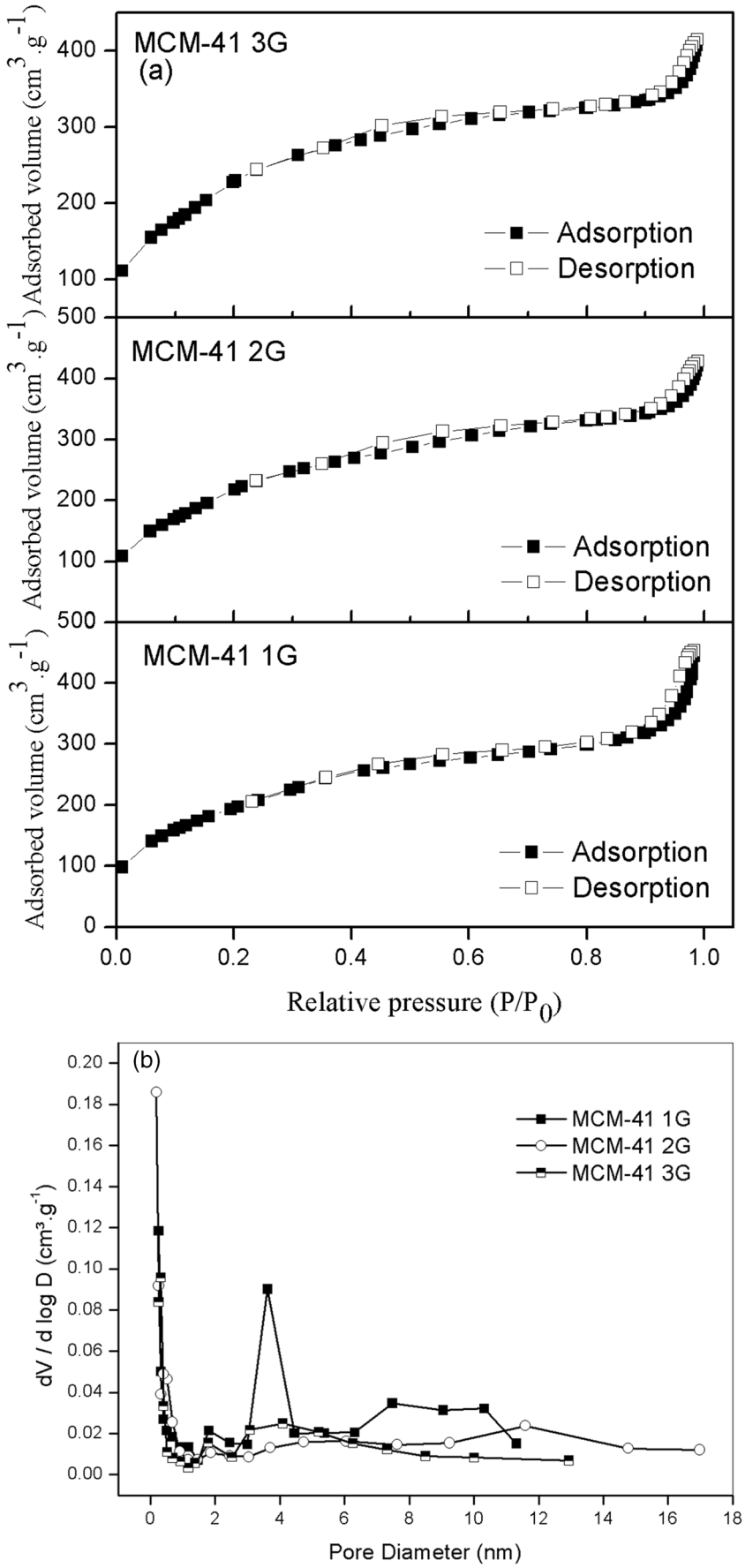

Fig. 5 Nitrogen adsorption-desorption isotherms (**a**). Pore size distributions (**b**)

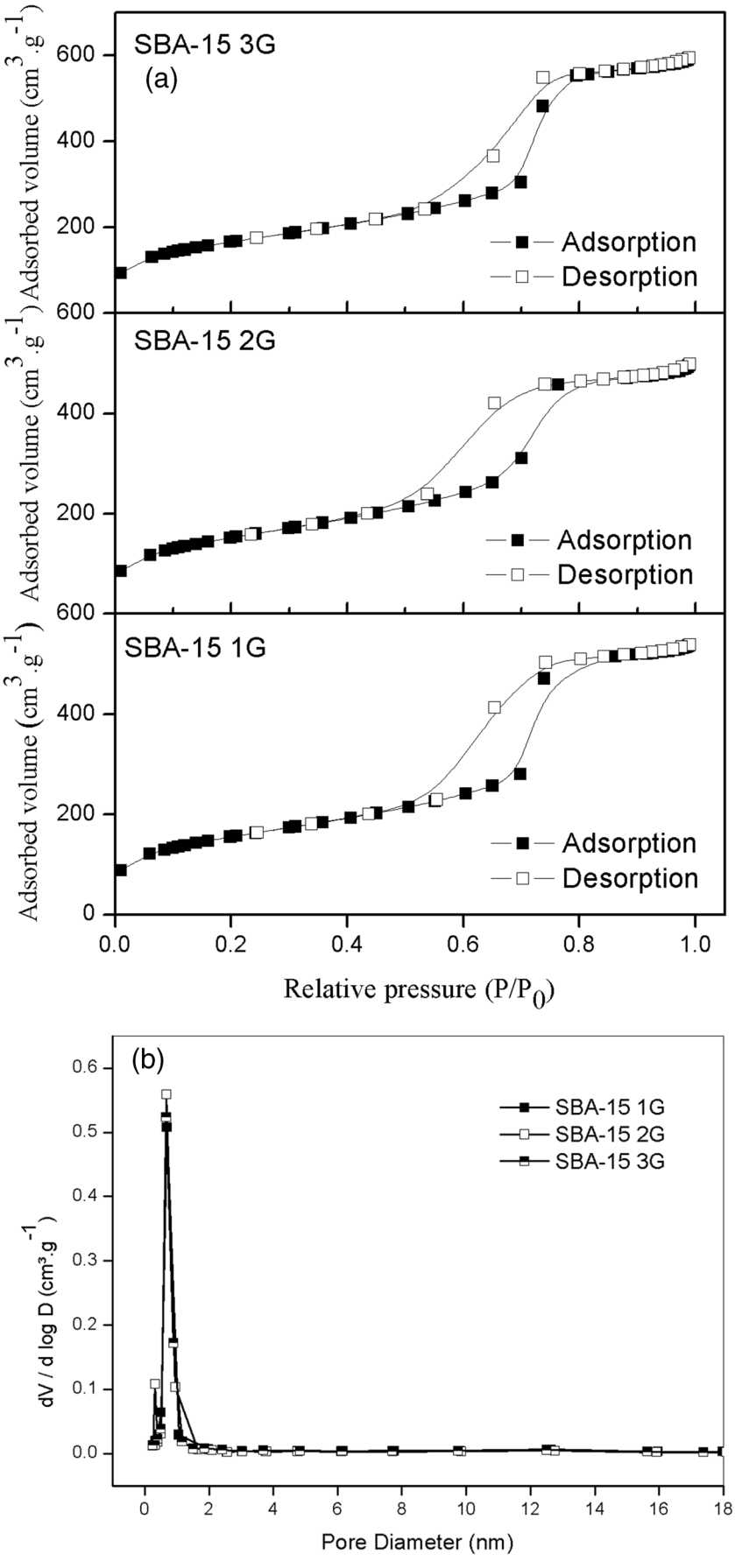

Fig. 6 Nitrogen adsorption-desorption isotherms SBA-15 (**a**). Pore size distributions (**b**)

Table 6 Synthesis parameters and characterization of the samples

	a_0 (nm)	S_{BET} ($m^2.g^{-1}$)	Dp BJH (nm)	Vp ($cm^3.g^{-1}$)	Wt (nm)
MCM-41 1G	4.87	726	3.53	0.64	1.34
MCM-41 2G	5.07	818	3.07	0.62	2.00
MCM-41 3G	5.02	867	2.80	0.63	2.22
SBA-15 1G	11.59	550	5.53	0.77	6.06
SBA-15 2G	11.92	561	5.92	0.83	6.00
SBA-15 3G	11.59	600	6.08	0.91	5.51

reaction, $C_{16}H_{33}(CH_3)_3\ N^+ \Rightarrow C_{16}H_{32} + N(CH_3)_3 + H^+$, contributes to about 31 % of the mass loss. And the third between 400 and 550 °C due to the residual removal of CTAB from the secondary condensation process of the silanol groups corresponding to 13 % of the total loss [22].

The thermogravimetric curves of the synthesized SBA-15 samples (Fig. 7(b)) indicate two mass loss events, the first below 100 °C with 5 % loss relative to the adsorption of physically adsorbed water and the second between 300 and 400 °C with 45 % of loss corresponding to the decomposition of the surfactant (Pluronic P123) occluded in the pores of the molecular sieve [43, 44]. These events can be observed in all samples SBA-15 and it is noticeable. Also a sharp peak of DTG between 300 and 400 °C regarding the elimination of surfactant P123 [45, 46].

The synthesized samples showed the three mass losses characteristic of the material mesoporous type MCM-41 and SBA-15. These results are shown in Table 7.

4 Conclusions

MCM-41 and SBA-15 silicas can be prepared more economically and ecologically by reusing unreacted reagents.

Crystals prepared from two subsequent batches of synthesis exhibit similar chemical composition and morphologies.

The synthesis process using the mother liquor was able to produce the structures of the mesoporous sieves MCM-41 and SBA-15 in the three generations, as determined by X-ray diffractograms (XRD), which showed characteristic peaks in the structure of these materials.

From the analysis of the textural characteristics of the various samples obtained through nitrogen adsorption/desorption studies carried out at -196 °C, the following important conclusions were highlighted: (i) For the synthesis of MCM-41, there was an increase in the specific surface area, reduced pore diameter and consequently increased wall thickness; (ii) For the synthesis of SBA-15 there was an increase in the specific

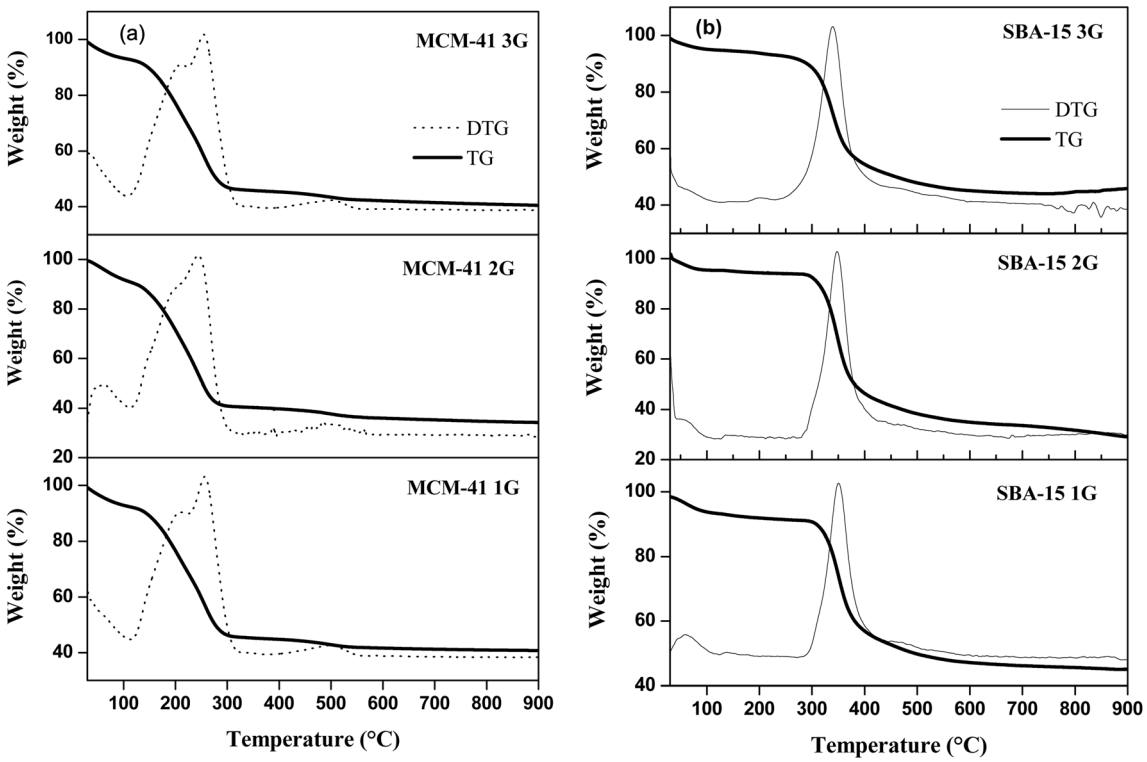

Fig. 7 TG/DTG curves for silica samples (**a**) MCM-41 (**b**) SBA-15

Table 7 Thermogravimetric analyses of the materials

Samples	Weight losses (%)						Total
	I		II		III		
	ΔT(ºC)	Δm(%)	ΔT(ºC)	Δm(%)	ΔT(ºC)	Δm(%)	
MCM-41 1G	25;151	11.13	151;320	43.28	320;898	4.86	59.27
MCM-41 2G	25;160	13.78	160;320	45.67	320;898	6.34	65.79
MCM-41 3G	25;150	10.50	150;320	43.29	320;898	5.75	59.54
SBA-15 1G	25;100	6.26	100;400	36.82	400;898	11.87	51.89
SBA-15 2G	25;100	4.58	100;400	49.03	400;897	17.31	68.03
SBA-15 3G	25;100	4.90	100;400	40.67	400;897	8.62	47.68

surface area, an increase in the pore diameter and, consequently, a reduction in the wall thickness.

This method of synthesis showed significant relevance in the reduction of effluents generated from the neutralization of the conventional synthesis of these silicas.

Acknowledgements The authors are grateful financial support provided by Coordenação de Aperfeiçoamento de Pessoal de NívelSuperior (CAPES).

Author Contributions Conceptualization, Thianne S. B. Barbosa and Thiago R. B. Barros; methodology, Thianne S. B. Barbosa and Thiago R. B. Barros; writing - original draft preparation, Thianne S. B. Barbosa; writing - review and editing, Tellys L. A. Barbosa and Meiry G. F. Rodrigues. All authors have read and agreed to the published version of the manuscript.

Funding This study was funded Coordenação de Aperfeiçoamento de Pessoal de Nível Superior (CAPES).

Data Availability Not applicable.

Declarations

Conflict of Interest The authors declare that they have no conflict of interest.

Not applicable.

Consent to Participate Not applicable.

Consent for Publication Not applicable.

References

1. Wang Y, Li L, Liu Y, Ren X, Liang J (2016) Antibacterial mesoporous molecular sieves modified with polymeric N-halamine. Mater Sci Eng C 69:1075–1080. https://doi.org/10.1016/j.msec.2016.08.017
2. Jaroszewska K, Masalska A, Czycz D, Grzechowiak J (2017) Activity of shaped Pt/AlSBA-15 catalysts in n-hexadecane hydroisomerization. Fuel Process Technol 167:1–10. https://doi.org/10.1016/j.fuproc.2017.06.012
3. Costa JAS, Jesus RA, Santos DO, Mano JF, Romão LPC, Paranhos CM (2020) Recent progresses in the adsorption of organic, inorganic, and gas compounds by MCM-41-based mesoporous materials. Microporous Mesoporous Mater 291:109698. https://doi.org/10.1016/j.micromeso.2019.109698
4. Wan Y, Zhao D (2009) Ordered mesopouros material. In: Jong KP (ed) Synthesis of solid catalyst. Wiley, Weinhein, pp 423
5. Meynen V, Coll P, Vansat EF (2009) Verified syntheses of mesoporous materials. Microporous Mesoporous Mater 125:170–223. https://doi.org/10.1016/j.micromeso.2009.03.046
6. Ying JY, Mehnert CP, Wong MS (1999) Synthesis and applications of Supramolecular-Templated Mesoporous Materials. Angew C Inter Ed 38:56–77. https://doi.org/10.1002/(sici)1521-3773(19990115)38:1/2<56::aid-anie56>3.0.co;2-e
7. Beck JS, Artuli JC, Roth WJ, Leonowicz ME, Kresge CT et al (1992) A new family of mesoporous molecular sieves prepared with liquid crystal templates. J Am Chem Soc 114:10834–10843. https://doi.org/10.1021/ja00053a020
8. Cai Q, Lin WY, Xiao FS, Pang WQ, Chen XH, Zou BS (1999) The preparation of highly ordered MCM-41 with extremely low surfactant concentration. Microporous Mesoporous Mater 32:1–15. https://doi.org/10.1016/s1387-1811(99)00082-7
9. Zhao E, Huo Q, Feng J, Chmelka BF, Stucky GD (1998) Nonionic triblock and star diblock copolymer and oligomeric surfactant syntheses of highly ordered, hydrothermally stable, mesoporous silica structures. J Am Chem Soc 120:6024–6036. https://doi.org/10.1021/ja974025i
10. Liu J, Yu J (2016) Toward greener and designed synthesis of zeolite materials. In: Zeolites and Zeolite-like Materials. https://doi.org/10.1016/b978-0-444-63506-8.00001-x
11. Duan F, Li J, Chen P, Yu J, Xu R (2009) A low-cost route to the syntheses of microporous cobalt-substituted aluminophosphates by using the waste mother-liquor. Microporous Mesoporous Mater 126:26–31. https://doi.org/10.1016/j.micromeso.2009.05.015
12. Liu Z, Li H, Zhang T, Wang Y et al (2020) Mother liquor induced preparation of SAPO-34 zeolite for MTO reaction. Catal Today 358:109–115. https://doi.org/10.1016/j.cattod.2020.03.034
13. Ghrear TMA, Ng EP, Vaulot C, Daou TJ, Ling TC, Tan SH, Ooi BS, Mintova S (2020) Recyclable synthesis of Cs-ABW zeolite nanocrystals from non-reacted mother liquors with excellent catalytic henry reaction performance. J Environ Chem Eng 8:103579. https://doi.org/10.1016/j.jece.2019.103579
14. Yang J, Huang Y-X, Pan Y, Mi J-X (2020) Green synthesis and characterization of zeolite silicalite-1 from recycled mother liquor. Microporous Mesoporous Mater 303:110247. https://doi.org/10.1016/j.micromeso.2020.110247

15. Sahin F, Topuz B, Kalipçilar H (2018) Synthesis of ZIF-7, ZIF-8, ZIF-67 and ZIF-L from recycled mother liquors. Microporous Mesoporous Mater 261:259–267. https://doi.org/10.1016/j.micromeso.2017.11.020
16. Zhong J, Han J, Wei Y, Tian P, Guo X, Song C, Liu Z (2017) Recent advances of the nano-hierarchical SAPO-34 in the methanol-to-olefin (MTO) reaction and other applications. Cat Sci Technol 7:4905–4923. https://doi.org/10.1039/c7cy01466j
17. Xi D, Sun Q, Chen X, Wang N, Yu J (2015) The recyclable synthesis of hierarchical zeolite SAPO-34 with excellent MTO catalytic performance. Chem Commun 51(60):11987–11989. https://doi.org/10.1039/c5cc03904e
18. Ng E-P, Goh J-Y, Ling TC, Mukti RR (2013) Eco-friendly synthesis for MCM-41 nanoporous materials using the non-reacted reagents in mother liquor. Nanoscale Res Lett 8:120. https://doi.org/10.1186/1556-276x-8-120
19. Chen TL, Kim H, Pan SY, Tseng PC, Lin YP, Chiang PC (2020) Implementation of green chemistry principles in circular economy system towards sustainable development goals: Challenges and perspectives. Sci Total Environ 716:136998. https://doi.org/10.1016/j.scitotenv.2020.136998
20. Anastas P, Eghbali N (2010) Green chemistry: principles and practice. Chem Soc Rev 39:301–312. https://doi.org/10.1039/b918763b
21. Lu D, Xu S, Qiu W, Sun Y, Liu X, Yang J, Ma J (2020) Adsorption and desorption behaviors of antibiotic ciprofloxacin on functionalized spherical MCM-41 for water treatment. J Clean Prod 264:121644. https://doi.org/10.1016/j.jclepro.2020.121644
22. Bezerra DM, Zapelini IW, Franke KN, Ribeiro ME, Cardoso D (2019) Investigation of the structural order and stability of mesoporous silicas under a humid atmosphere. Mater Charact 154:103–115. https://doi.org/10.1016/j.matchar.2019.05.032
23. Adrover ME, Pedernera M, Bonne M, Lebeau B, Bucalá V, Gallo L (2020) Synthesis and characterization of mesoporous SBA-15 and SBA-16 as carriers to improve albendazole dissolution rate. Saudi Pharma J 28:15–24. https://doi.org/10.1016/j.jsps.2019.11.002
24. Marinho JC, Barbosa TLA, Rodrigues MGF (2018) Preparation of molecular sieve Al-SBA-15 with two ratios Si/Al catalyst for use in the transesterification reaction of soybean oil. Mater Sci Forum 912:39–43. https://doi.org/10.4028/www.scientific
25. Wijaya DP, Trisunaryanti W, Dewi TK, Marsuki MF (2018) Synthesis and characterization Of K_2O/MCM-41 (Mobil Composition of Matter No. 41) from lapindo mud by sonochemical method for transesterification catalyst of used cooking oil. Orient J Chem 34(4):1847–1853. https://doi.org/10.13005/ojc/3404019
26. Cotea VV, Luchian CE, Bilba N, Niculaua M (2012) Mesoporous silica SBA-15. a new adsorbent for bioactive polyphenols from red wine. Anal Chim Acta 732:180–185. https://doi.org/10.1016/j.aca.2011.10.019
27. Koh CA, Nooney R, Tahir S (1997) Characterization and catalytic properties of MCM-41 and Pd/MCM-41 materials. Catal Lett 47:199–205. https://doi.org/10.1023/A:1019025609426
28. Zholobenko V, Garforth A, Dwyer J (1997) TGA-DTA study on calcination of zeolitic catalysts. Thermo Acta 294:39–44. https://doi.org/10.1016/s0040-6031(96)03140-1
29. Holmes SM, Zholobenko VL, Thursfield A, Plaisted RJ, Cundy CS, Dwyer J (1998) In situ FTIR study of the formation of MCM-41. J Chem Soc Faraday Trans 94:2025–2032. https://doi.org/10.1039/a801898g
30. Marinescu G, Culita DC, Romanitan C, Somacescu S et al (2020) Novel hybrid materials based on heteroleptic Ru(III) complexes immobilized on SBA-15 mesoporous silica as highly potent antimicrobial and cytotoxic agents. Appl Surf Sci 520:146379. https://doi.org/10.1016/j.apsusc.2020.146379
31. Wang X, Chan JCC, Tseng YH, Cheng S (2006) Synthesis, characterization and catalytic activity of ordered SBA-15 materials containing high loading of diamine functional groups. Microporous Mesoporous Mater 78:58–65. https://doi.org/10.1016/j.micromeso.2006.05.003
32. Siverstein RW, Bassler GC (1962) Spectrometric Identification of Organic Compounds. J Chem Educ 39:546–553. https://doi.org/10.1021/ed039p546
33. Stuart BH (2004) Infrared spectroscopy: fundamentals and applications. Wiley, Hoboken
34. Kresge CT, Leonowicz ME, Roth WJ, Vartuli JC, Beck JS (1992) Ordered mesoporous molecular sieves synthesized bay a liquid-crystal template mechanism. Nature 359:710–712. https://doi.org/10.1038/359710a0
35. Grün M, Unger KK, Matsumoto A, Tsutsumi K (1999) Novel pathways for the preparation of mesoporous MCM-41 materials control of porosity and morphology. Microporous Mesoporous Mater 27:207–2016. https://doi.org/10.1016/s1387-1811(98)00255-8
36. Ferrer DM, Banda JAM, Rodrigo RS, García UP, Gómez JYV, Vicente PDA (2018) Synthesis of micro/nanostructured carbon from refined sugar and its electrochemical performance. Inter J Electrochem Sci 13:708–718. https://doi.org/10.20964/2018.01.65
37. Katiyar A, Yadav S, Smirniotis PG, Pinto NG (2006) Synthesis of ordered large pore SBA-15 spherical particles for adsorption of biomolecules. J Chromatogr 1122:13–20. https://doi.org/10.1016/j.chroma.2006.04.055
38. Chao MC, Lin HP, Sheu HS, Mou CY (2002) A study of morphology of mesoporous silica SBA- 15. Stud Surf Sci Catal 141:387–394
39. IUPAC Recommendations (1985) Pure Appl Chem 57:603–619
40. Lin YW, Cheng TW, Lo KW, Chen CY, Lin KL (2020) Synthesis and characterization of a mesoporous Al-MCM-41 molecular sieve material and its moisture regulation performance in water molecule adsorption/desorption. Microporous Mesoporous Mater 310:110643. https://doi.org/10.1016/j.micromeso.2020.110643
41. Yin Y, Wen Z-H, Liu X-Q, Yuan A-H, Shi L (2017) Functionalization of SBA-15 with CeO_2 nanoparticles for adsorptive desulfurization: Matters of template P123. Adsorpt Sci Technol. https://doi.org/10.1177/0263617417734767
42. Rodrigues JJ, Fernandes FAN, Rodrigues MGF (2013) Study of Co/SBA-15 catalysts prepared by microwave and conventional heating methods and application in Fischer-Tropsch synthesis. Appl Catal A 468:32–37. https://doi.org/10.1016/j.apcata.2013.08.035
43. Janus R, Wadrzyk M, Lewandowski M, Natkanski P, Latka P, Kustrowaki P (2020) Understanding porous structure of SBA-15 upon pseudomorphic transformation into MCM-41: Non-direct investigation by carbon replication. J Ind Eng Chem 92:131–144. https://doi.org/10.1016/j.jiec.2020.08.032
44. Janus R, Wadrzyk M, Natkanski P, Cool P, Kustrowaki P (2019) Dynamic adsorption-desorption of methyl ethyl ketone on MCM-41 and SBA-15 decorated with thermally activated polymers. J Ind Eng Chem 71:465–480. https://doi.org/10.1016/j.jiec.2018.12.004
45. Deng X, Chen K, Tuysuz H (2017) Protocol for the nanocasting method: preparation of ordered mesoporous metal oxides. Chem Mater 29:40–52. https://doi.org/10.1021/acs.chemmater.6b02645
46. Serrano DP, Calleja G, Botas JA, Gutierrez FJ (2004) Adsorption and hydrophobic properties of mesostructured MCM-41 and SBA-15 materials for volatile organic compound removal. Ind Eng Chem Res 43:7010–7018. https://doi.org/10.1021/ie040108d